Electronic Supplementary Information

Tuning the d-band center of NiC_2O_4 with Nb_2O_5 to optimize the Volmer step for hydrazine oxidation-assisted hydrogen production

Xiao Hui Chen [a], Hong Chuan Fu [a], Li Li Wu [a], Xiao Lin Li [a], Bo Yang [a], Ting Li [a], Fei Gu [a], Jing Lei Lei [b], Nian Bing Li [a],*, Hong Qun Luo [a],*

[a] School of Chemistry and Chemical Engineering, Southwest University, Chongqing 400715, People's Republic of China

[b] School of Chemistry and Chemical Engineering, Chongqing University, Chongqing 400044, People's Republic of China

*Corresponding author.

Nian Bing Li and Hong Qun Luo

E-mail address: linb@swu.edu.cn; luohq@swu.edu.cn

Experimental Section

Material and reagent: Niobium pentachloride ($NbCl_5$), ethylenediamine solution (EDA), and thiourea (CH_4N_2S) were manufactured by Aladdin Co., Ltd. (Shanghai, China), Yuexiang Chemical Co., Ltd. (Chongqing, China), and Macklin Co., Ltd. (Chengdu, China), respectively. Nafion (5 wt %) and oxalic acid ($H_2C_2O_4$) were purchased from Sigma-Aldrich (Chongqing, China). The potassium hydroxide (KOH) used in this work was produced in Chuandong Chemical Co., Ltd. (Chengdu, China). Ni foam (NF) was purchased from Cyber Electrochemistry (Beijing, China).

Electrochemical performance: All electrochemical parameters of the synthesized catalysts were obtained from CHI 660E electrochemical workstation. A graphite rod, Ag/AgCl (KCl saturated) and $SNiC_2O_4$-Nb_2O_5/NF (0.5 cm^2) were served as the counter, reference and working electrodes, respectively. The electrochemical impedance spectroscopy (EIS) was recorded in the frequency range from 1 MHz to 0.01 Hz (η = 127 mV for HER and η = 343 mV for OER). The OWS performance was tested in a two-electrode system using $SNiC_2O_4$-Nb_2O_5/NF as the catalyst. The obtained potentials were all converted into reversible hydrogen electrode (RHE) on the basis of Nernst equation. The polarization curve was obtained at a scan rate of 5 mV s^{-1} in 1.0 M KOH or 1.0 M KOH/0.5 M N_2H_4.

The amounts of generated H_2, O_2 and N_2 were collected in the H-type of the electrolytic cell using the drainage method. The Faraday efficiency (FE) was acquired according to the following formula：

$$FE = z \times n \times \frac{F}{I \times t} \times 100\%$$

Eq. (1)

where z is the electron transfer number, n is the amount (moles) of the generated gas in the experiment, F is the Faraday constant (96485.3 C mol^{-1}), I is the applied constant current (A), and t is the electrolysis time (s).

Characterization: The morphology of the obtained materials was observed by scanning electron microscopy (SEM, ZEISS Gemini 300, ZEISS, Germany) and transmission electron microscopy (TEM, Tecnai G220, Fei Corporation, Japan). The crystalline structures of samples were identified by powder X-ray diffraction (XRD, X' Pert PRO, PANalytical B.V., Holland) using Cu-Kα radiation. The Raman spectra were measured on a Horiba Scientific LabRAM HR Evolution (HORIBA Jobin Yvon, France). The laser power used in Raman is 1.5 mW, and the radiation time is 30 s. The X-ray photoelectron spectroscopy (XPS) analysis was measured on Thermo Scientific K-Alpha using Mg-Kα radiation (Thermoelectricity Instruments, USA).

Computational methods: We employed the Vienna Ab Initio Package (VASP) [1, 2] to perform all the density functional theory (DFT) calculations within the Generalized Gradient Approximation (GGA) using the Perdew-Burke-Ernzerhof (PBE) formulation [3]. We chose the projected augmented wave (PAW) potentials [4, 5]. to describe the ionic cores and took valence electrons into account using a plane wave basis set with a kinetic energy cutoff of 400 eV. Partial occupancies of the Kohn−Sham orbitals were allowed using the Gaussian smearing method and a width of 0.05 eV. The electronic energy was considered self-consistent when the energy change was smaller than 10^{-5} eV. A geometry optimization was considered convergent when the force change was smaller than 0.05 eV/Å. Grimme's DFT-D3 methodology [6] was used to describe the dispersion interactions. The vacuum spacing perpendicular to the plane of the structure is 15 Å. The Brillouin zone integral uses the surface structures of 2×2×1 monkhorst pack K point sampling. Nb_2O_5 (001) and NiC_2O_4 (-202)

surfaces had been established in our systems. Finally, the adsorption energies (E_{ads}) are calculated by the following formula:
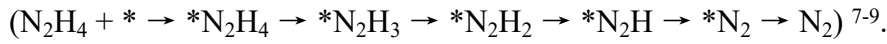
$$E_{ads} = E_{ad/sub} - E_{ad} - E_{sub} \qquad \text{Eq. (2)}$$

where $E_{ad/sub}$, E_{ad}, and E_{sub} are the optimized adsorbate/substrate system, the adsorbate in the structure, and the clean substrate, respectively. The free energy is calculated as follows:

$$G = E + ZPE - TS \qquad \text{Eq. (3)}$$

where G, E, ZPE, and TS are the free energy, total energy from DFT calculations, zero point energy, and entropic contributions, respectively.

The mechanism of HzOR: It is known that the hydrazine oxidation process involves six steps

$(N_2H_4 + * \rightarrow *N_2H_4 \rightarrow *N_2H_3 \rightarrow *N_2H_2 \rightarrow *N_2H \rightarrow *N_2 \rightarrow N_2)$ [7-9].

(A) $* + N_2H_4 \rightarrow *N_2H_4$ \qquad Eq. (4)

(B) $*N_2H_4 \rightarrow *N_2H_3 + H^+ + e^-$ \qquad Eq. (5)

(C) $*N_2H_3 \rightarrow *N_2H_2 + H^+ + e^-$ \qquad Eq. (6)

(D) $*N_2H_2 \rightarrow *N_2H + H^+ + e^-$ \qquad Eq. (7)

(E) $*N_2H \rightarrow *N_2 + H^+ + e^-$ \qquad Eq. (8)

(F) $*N_2 \rightarrow * + N_2$ \qquad Eq. (9)

The asterisk (*) represents the active sites. The rate-determining step of the reaction process depends on the characteristics of the catalyst, and is generally the step of forming N_2H_2 or N_2H.
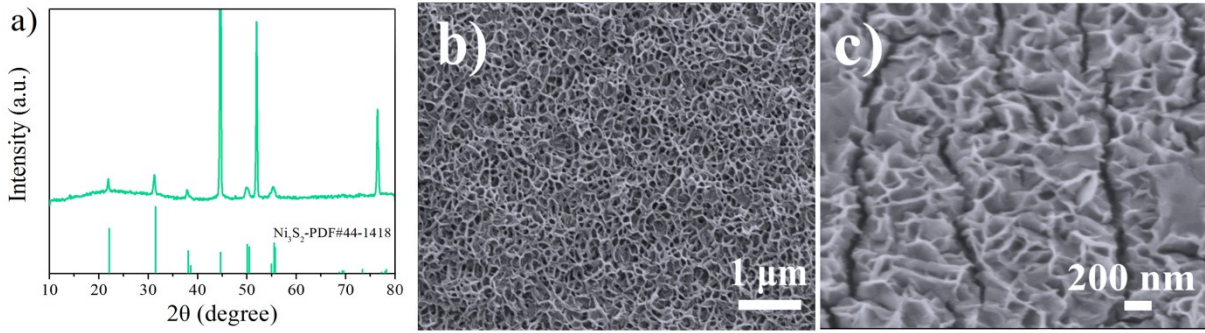
Fig. S1. a) XRD pattern and b-c) SEM images of Ni_3S_2.
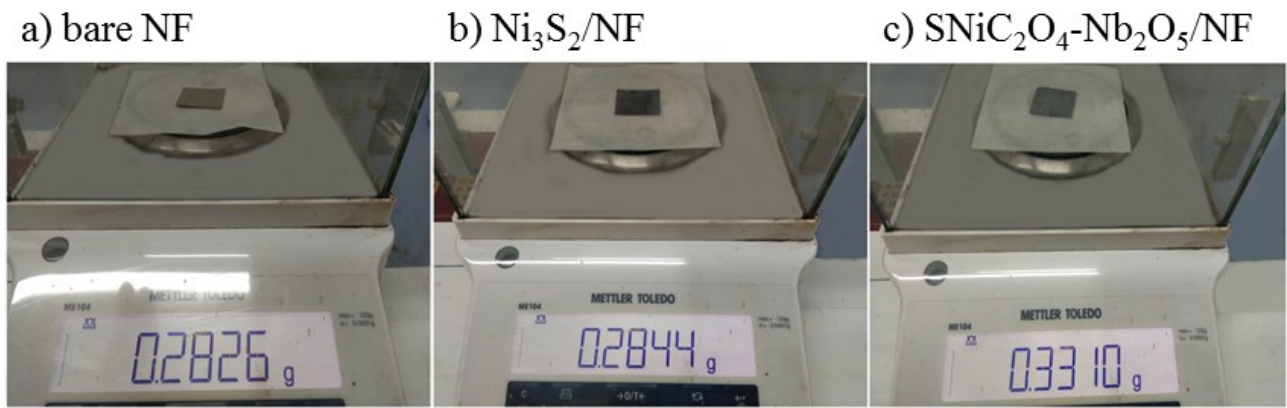
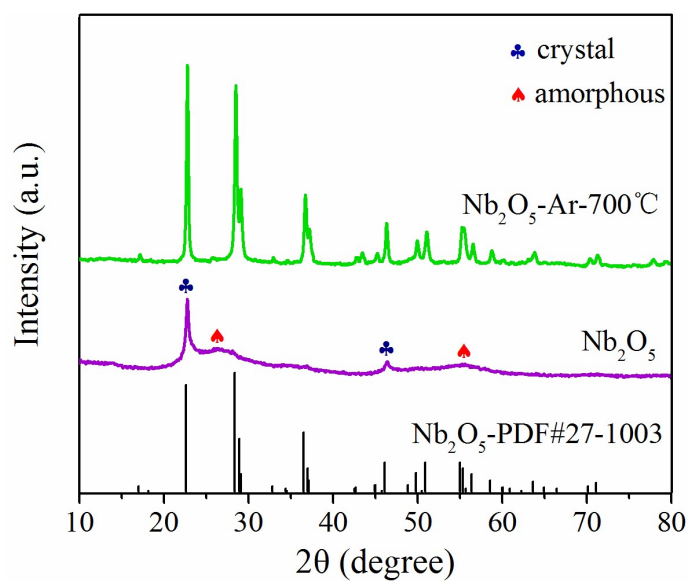**Fig. S2.** The mass of a) bare NF (m_1, 0.2826 g), b) Ni_3S_2/NF (m_2, 0.2844 g), and c) $SNiC_2O_4$-Nb_2O_5/NF (m_3, 0.3310 g).

The loading mass (Δm) of $SNiC_2O_4$-Nb_2O_5 on NF is calculated as follows:
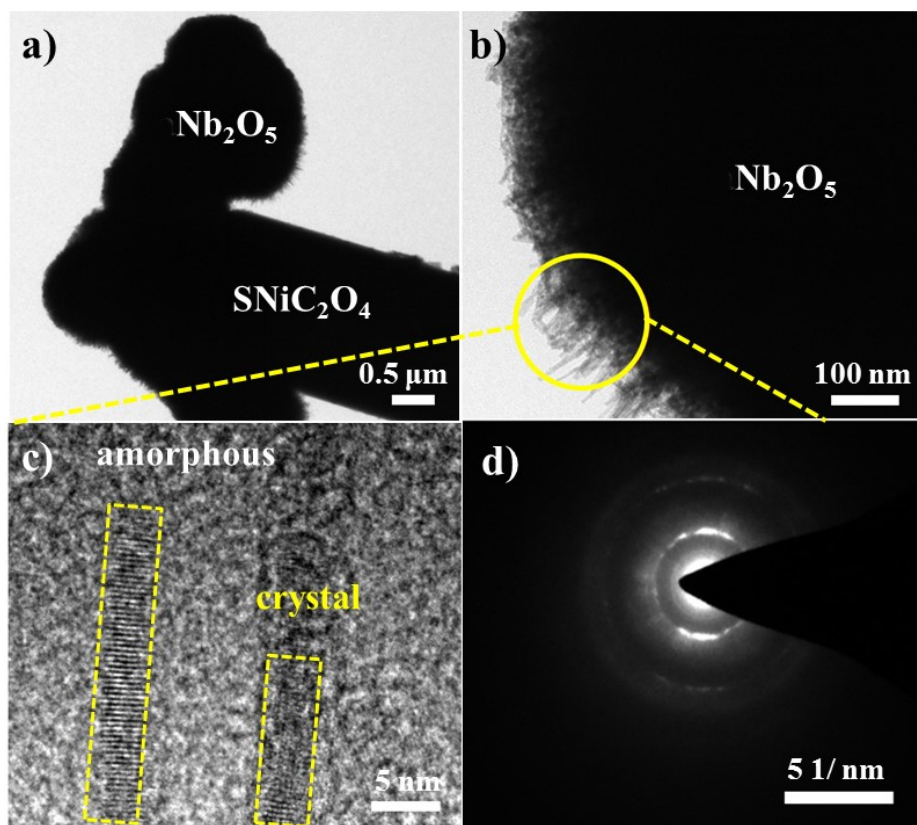
$$\Delta m = (m_3 - m_1) / A \qquad \text{Eq. (10)}$$

where A is the area of NF (A = 3 cm × 3 cm). Thus, Δm of $SNiC_2O_4$-Nb_2O_5 on NF is calculated to be 5.4 mg cm^{-2}
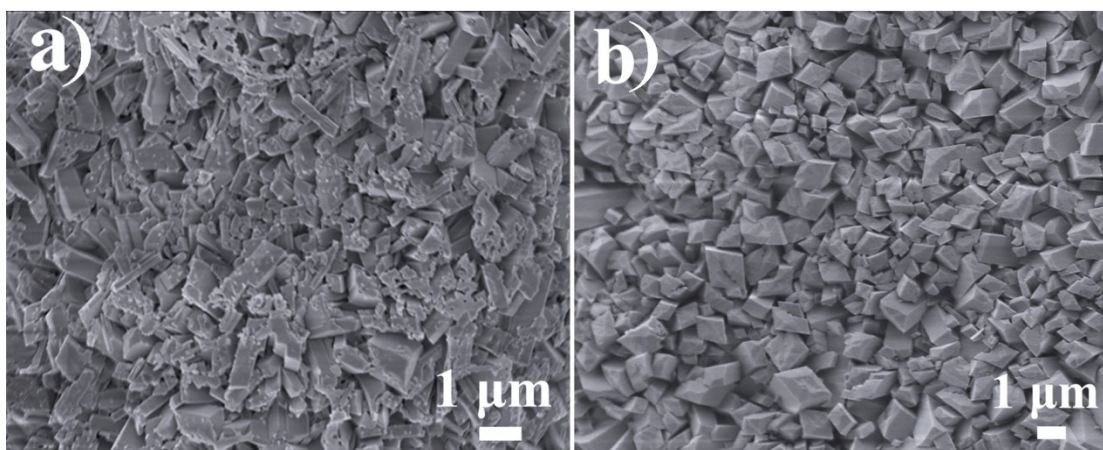
**Fig. S3.** SEM images of a) NiC_2O_4 and b) $SNiC_2O_4$.

Fig. S4. XRD patterns of Nb_2O_5 and the sample obtained by calcination of Nb_2O_5 at 700°C for 1 hour under the protection of Ar.

Fig. S5. a) TEM image of $SNiC_2O_4$-Nb_2O_5, b) TEM, c) high-resolution TEM and d) selected area electron diffraction (SAED) images of Nb_2O_5.
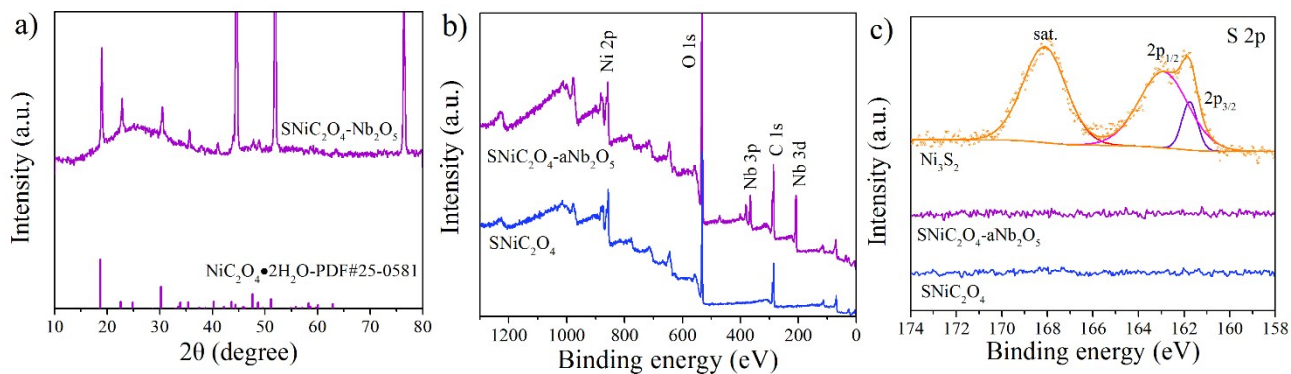
Fig. S6. a) XRD and b) XPS full survey spectra of SNiC$_2$O$_4$-Nb$_2$O$_5$ and SNiC$_2$O$_4$. c) S 2p survey spectra of Ni$_3$S$_2$, SNiC$_2$O$_4$ and SNiC$_2$O$_4$-Nb$_2$O$_5$.
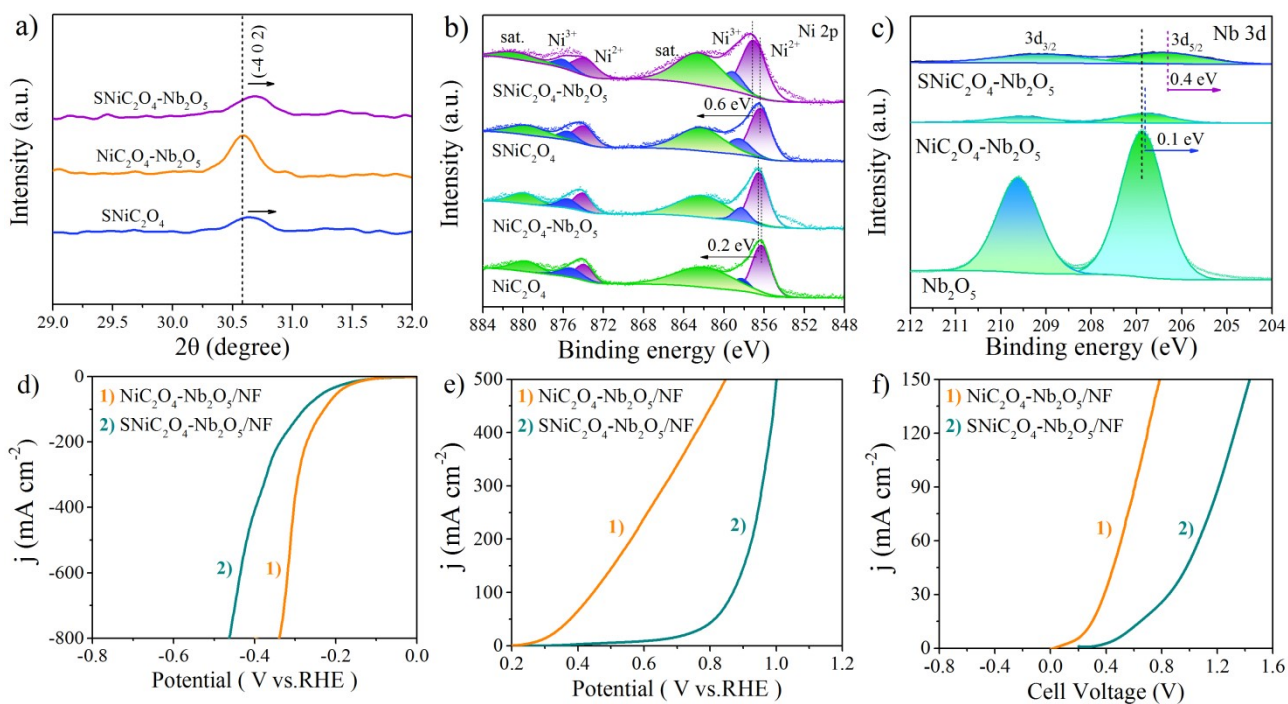
Fig. S7. a) The XRD peak of (-402) for SNiC$_2$O$_4$-Nb$_2$O$_5$, NiC$_2$O$_4$-Nb$_2$O$_5$, and SNiC$_2$O$_4$. Comparison of b) Ni and c) Nb XPS spectral data of the as-prepared catalysts. LSV curves of SNiC$_2$O$_4$-Nb$_2$O$_5$/NF and NiC$_2$O$_4$-Nb$_2$O$_5$/NF for d) HER, e) HzOR, and f) OHzS.

Table S1. Summary of deconvoluted XPS peaks of the as-prepared catalysts for Ni 2p.

Catalyst	$2p_{1/2}$ (eV)			$2p_{3/2}$ (eV)		
	sat.	Ni^{3+}	Ni^{2+}	sat.	Ni^{3+}	Ni^{2+}
$SNiC_2O_4$-Nb_2O_5	880.6	875.9	873.8	862.5	859.1	857.0
$SNiC_2O_4$	879.5	875.5	873.9	862.3	858.5	856.4
NiC_2O_4-Nb_2O_5	879.9	875.6	874.0	862.2	858.3	856.5
NiC_2O_4	879.7	875.2	873.9	862.0	858.3	856.3

Table S2. Summary of deconvoluted XPS peaks of the as-prepared catalysts for Nb 3d.

Catalyst	$3d_{3/2}$ (eV)	$3d_{5/2}$ (eV)
$SNiC_2O_4$-Nb_2O_5	209.1	206.4
NiC_2O_4-Nb_2O_5	209.5	206.8
Nb_2O_5	209.6	206.9
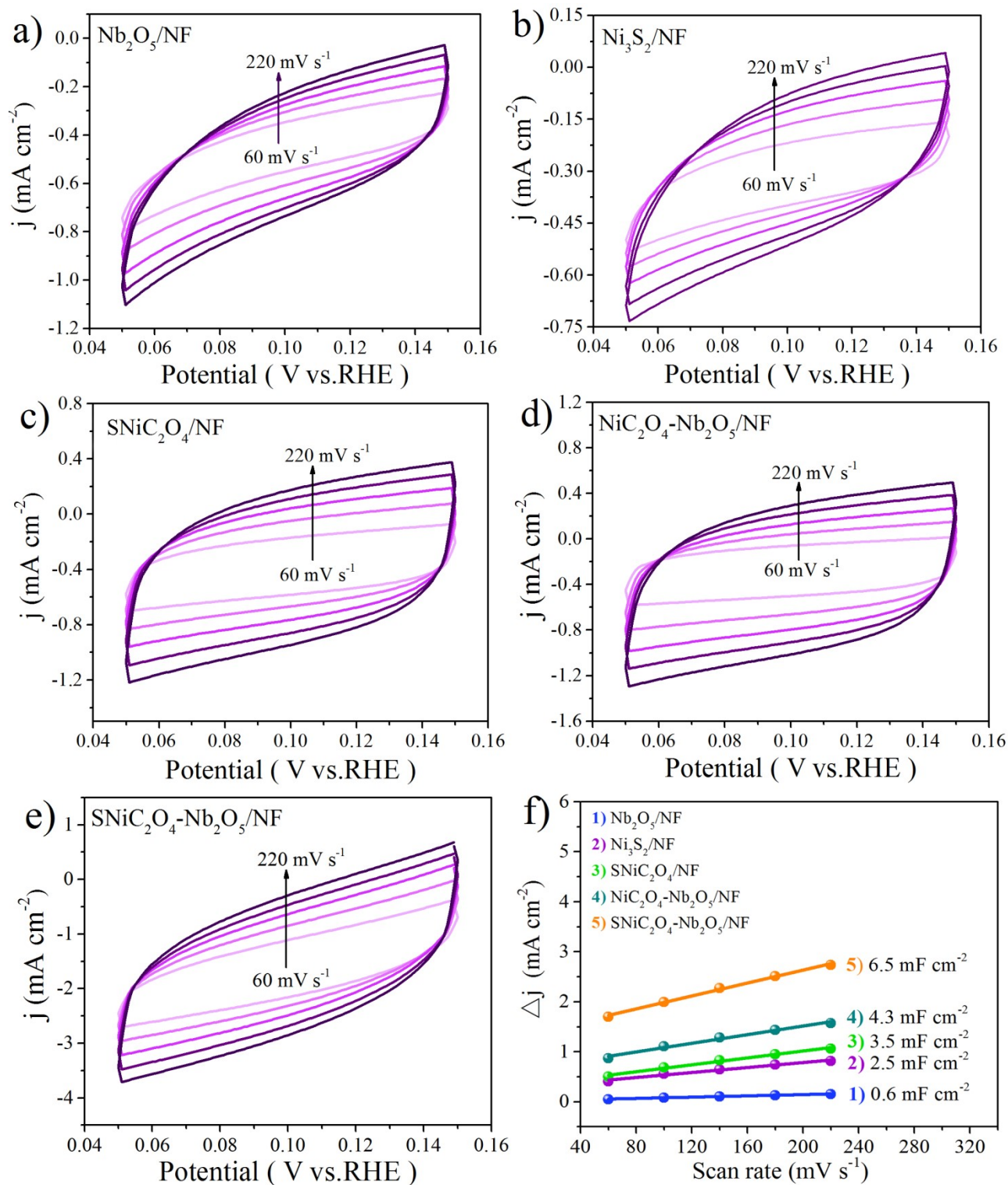
Fig. S8. CV curves of a) Nb_2O_5/NF, b) Ni_3S_2/NF, c) $SNiC_2O_4$/NF, d) NiC_2O_4-Nb_2O_5/NF, and e) $SNiC_2O_4$-Nb_2O_5/NF measured in 1.0 M KOH solution at scan rates from 60 to 220 mV s^{-1}. f) The capacitive current at 0.10 V vs. RHE of the as-prepared catalysts.

The double layered capacitance (C_{dl}) of $SNiC_2O_4$-Nb_2O_5/NF is the biggest, thus the catalytically relevant surface area for HER is the highest, mainly due to its more exposed active sites. The electrochemical surface area (ECSA) of $SNiC_2O_4$-Nb_2O_5/NF was estimated from their C_{dl} values, which have been measured using simple cyclic voltammetry method. Here the potential window has been chosen outside the possible Faradic region of the hybrid. Then the current is only generated for charging of double layer which is expected to have a linear relationship with the active surface area. The relationship between the capacitive current density, Δj ($\Delta j = j_{anodic} - j_{cathodic}$ at 0.10 V vs. RHE), and the scan rate is linear and the double layer capacitance (C_{dl}) has been calculated from the slope.
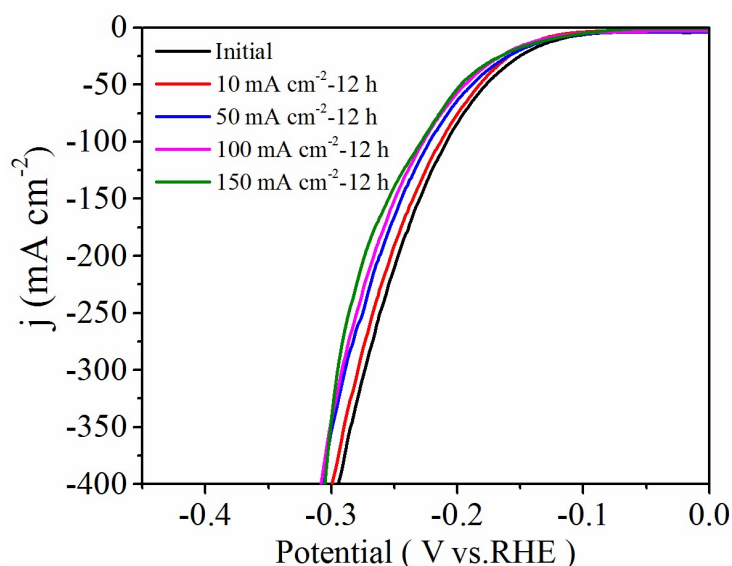
**Fig. S9.** LSV curves of $SNiC_2O_4$-Nb_2O_5/NF before and after maintaining the current density at -10, -50, -100, -150 mA cm^{-2} for 12 h in HER.
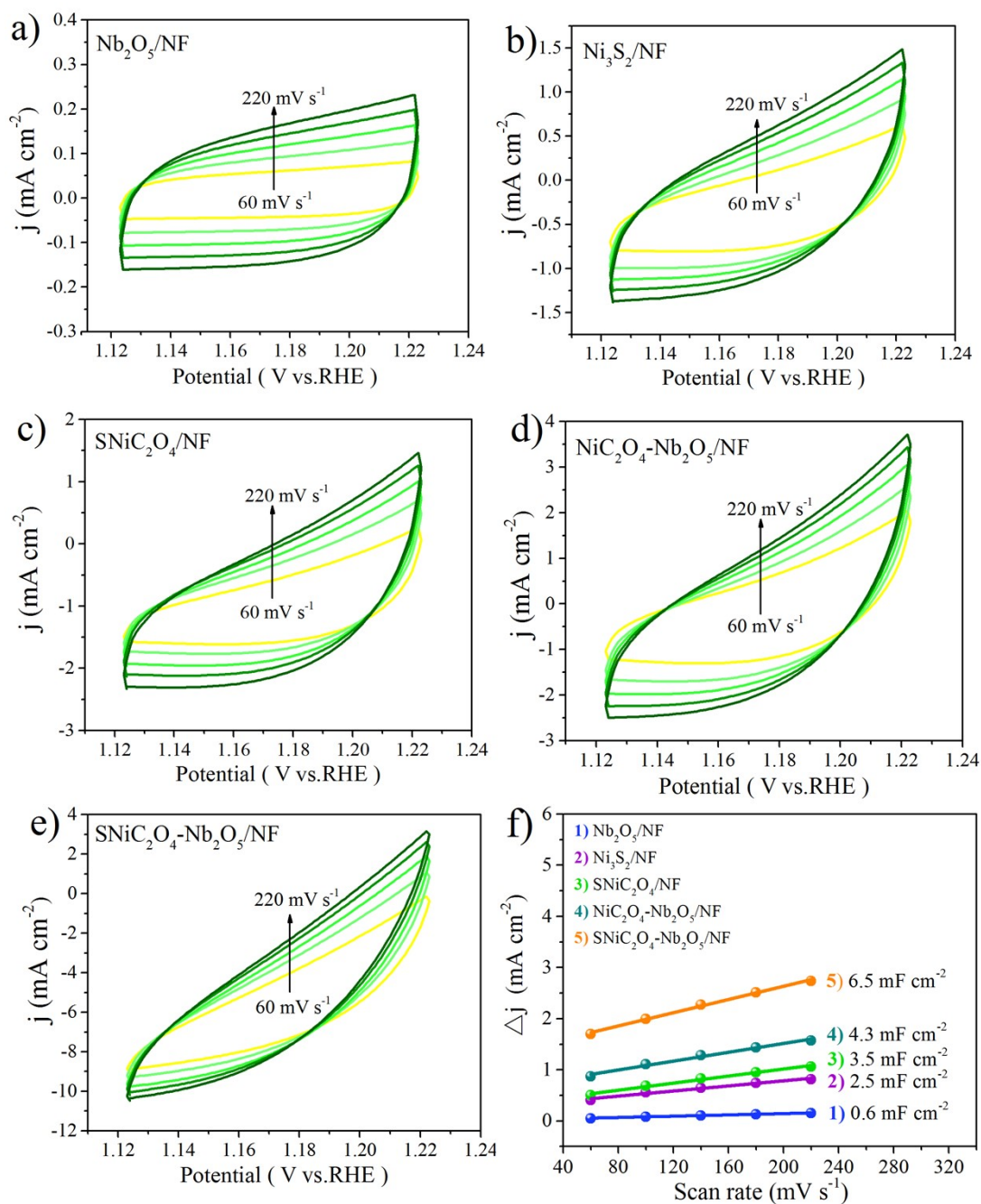
Fig. S10. CV curves of a) Nb_2O_5/NF, b) Ni_3S_2/NF, c) $SNiC_2O_4$/NF, d) NiC_2O_4-Nb_2O_5/NF and e) $SNiC_2O_4$-Nb_2O_5/NF measured in 1.0 M KOH solution at scan rates from 60 to 220 mV s^{-1}. f) The capacitive current at 1.18 V *vs.* RHE of the as-prepared catalysts.
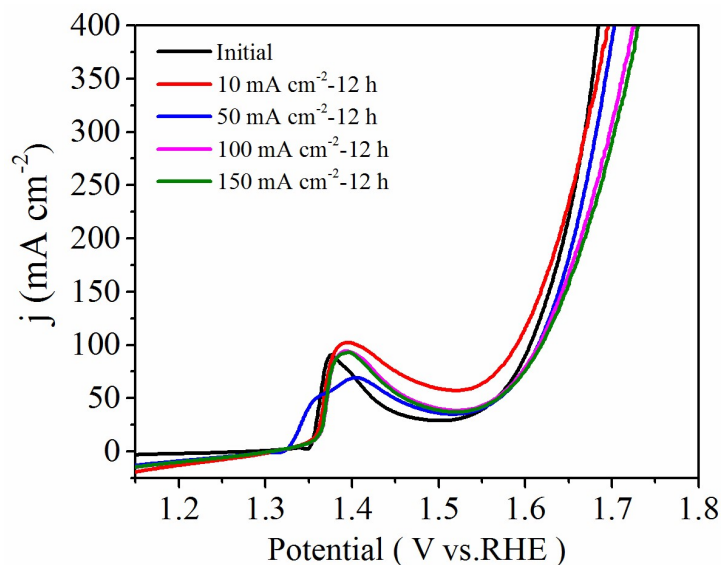
Fig. S11. LSV curves of SNiC$_2$O$_4$-Nb$_2$O$_5$/NF before and after maintaining the current density at 10, 50, 100, 150 mA cm^{-2} for 12 h in OER.
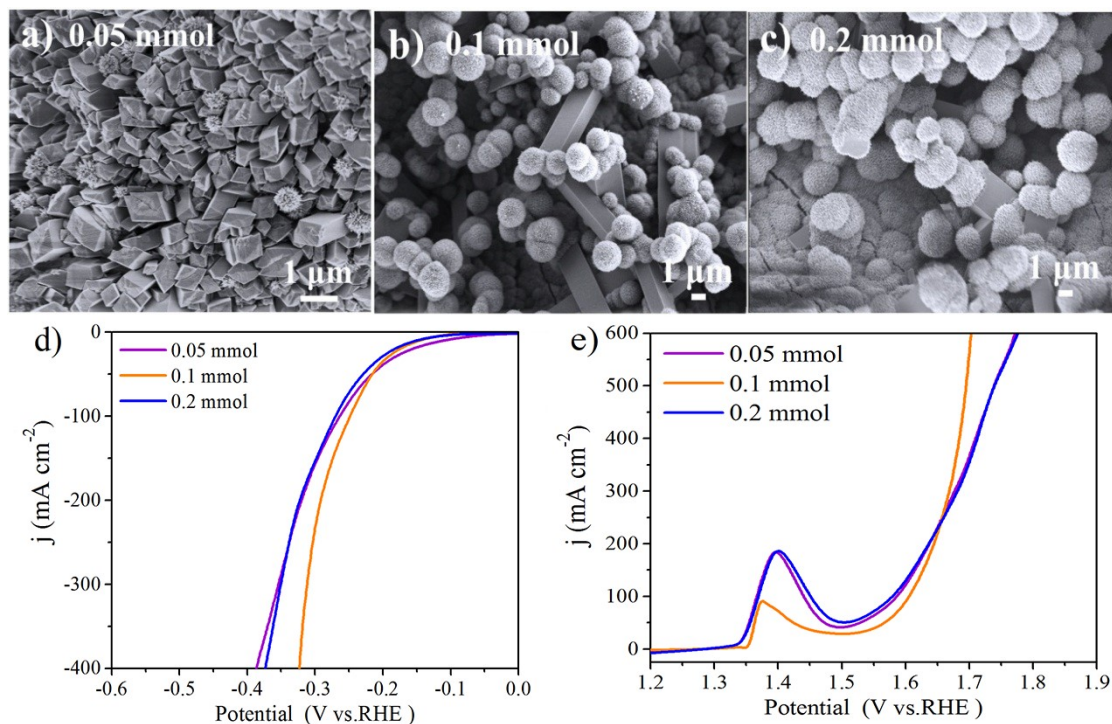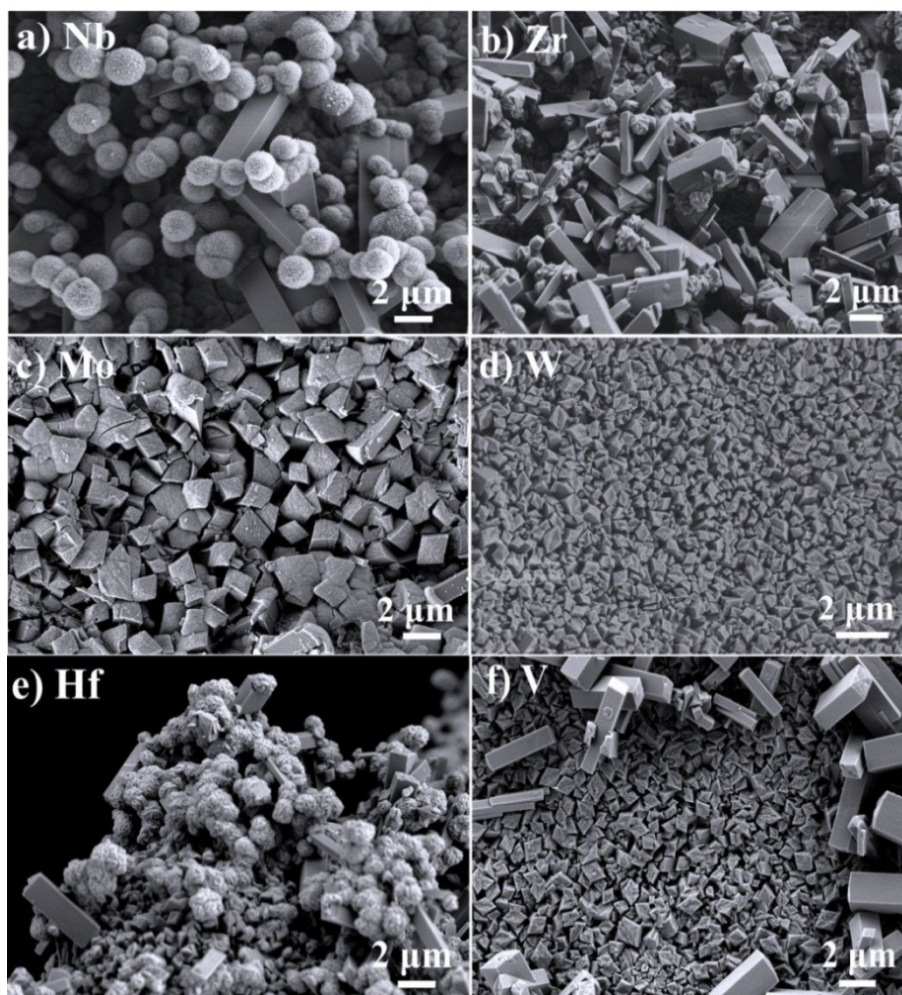

Fig. S12. SEM image of SNiC$_2$O$_4$-Nb$_2$O$_5$ prepared by adding a) 0.05 mol, b) 0.1 mol and b) 0.2 mol of Nb^{5+} in the hydrothermal process. d) HER and e) OER polarization curves of the above catalysts.
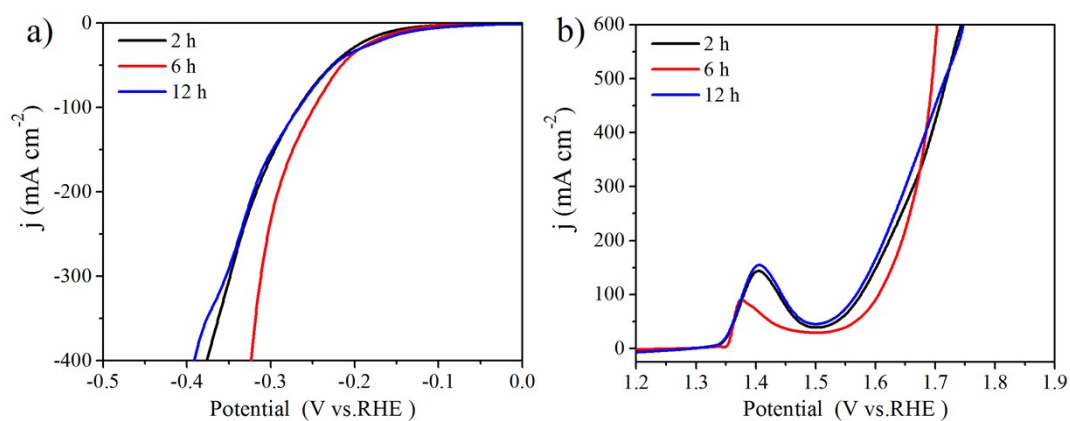
Fig. S13. HER a) and OER b) polarization curves of SNiC$_2$O$_4$-Nb$_2$O$_5$ at different hydrothermal reaction times.

Fig. S14. SEM images of the catalysts prepared by adding 0.1 mmol of a) NbCl$_5$, b) ZrCl$_4$, c) MoCl$_5$, d) WCl$_6$, e) HfCl$_4$, and f) VCl$_3$ in the hydrothermal process.
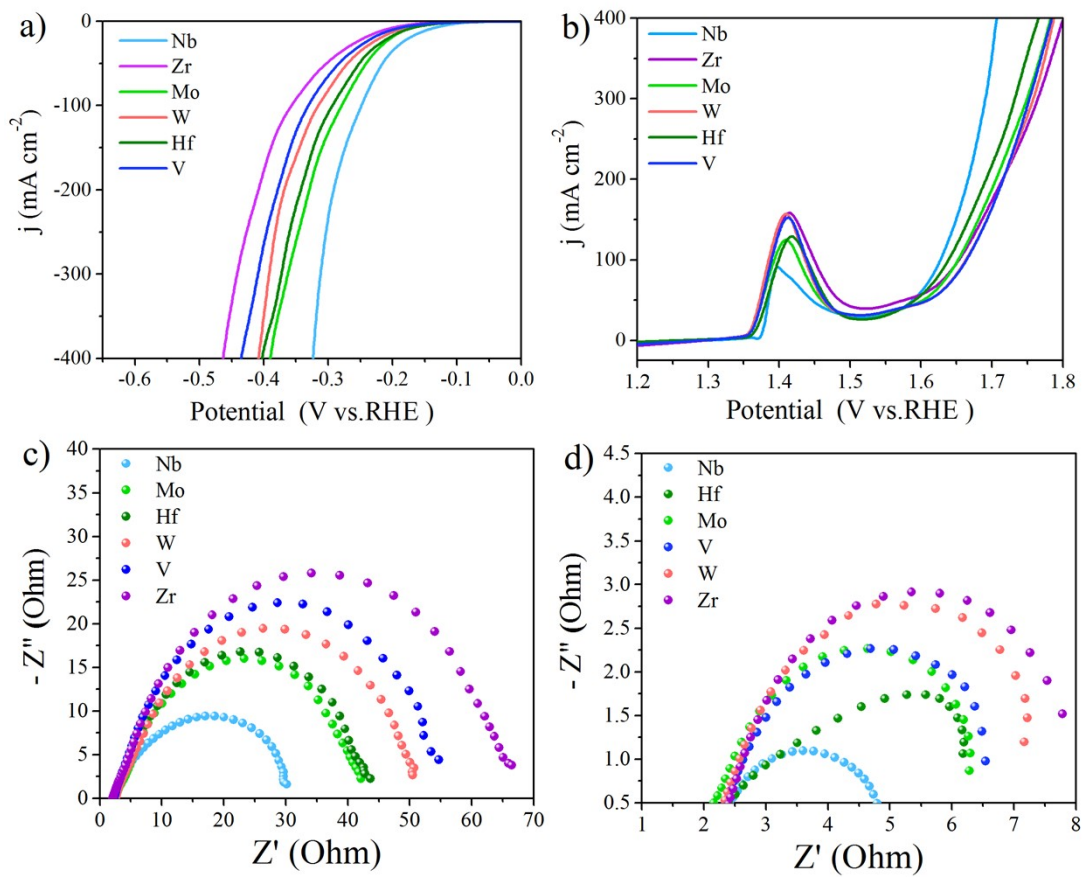
Fig. S15. a) HER and b) OER polarization curves of the catalysts prepared by adding 0.1 mmol of NbCl$_5$, ZrCl$_4$, MoCl$_5$, WCl$_6$, HfCl$_4$, and VCl$_3$ in the hydrothermal process. EIS profiles of the above catalysts in c) HER and d) OER processes.
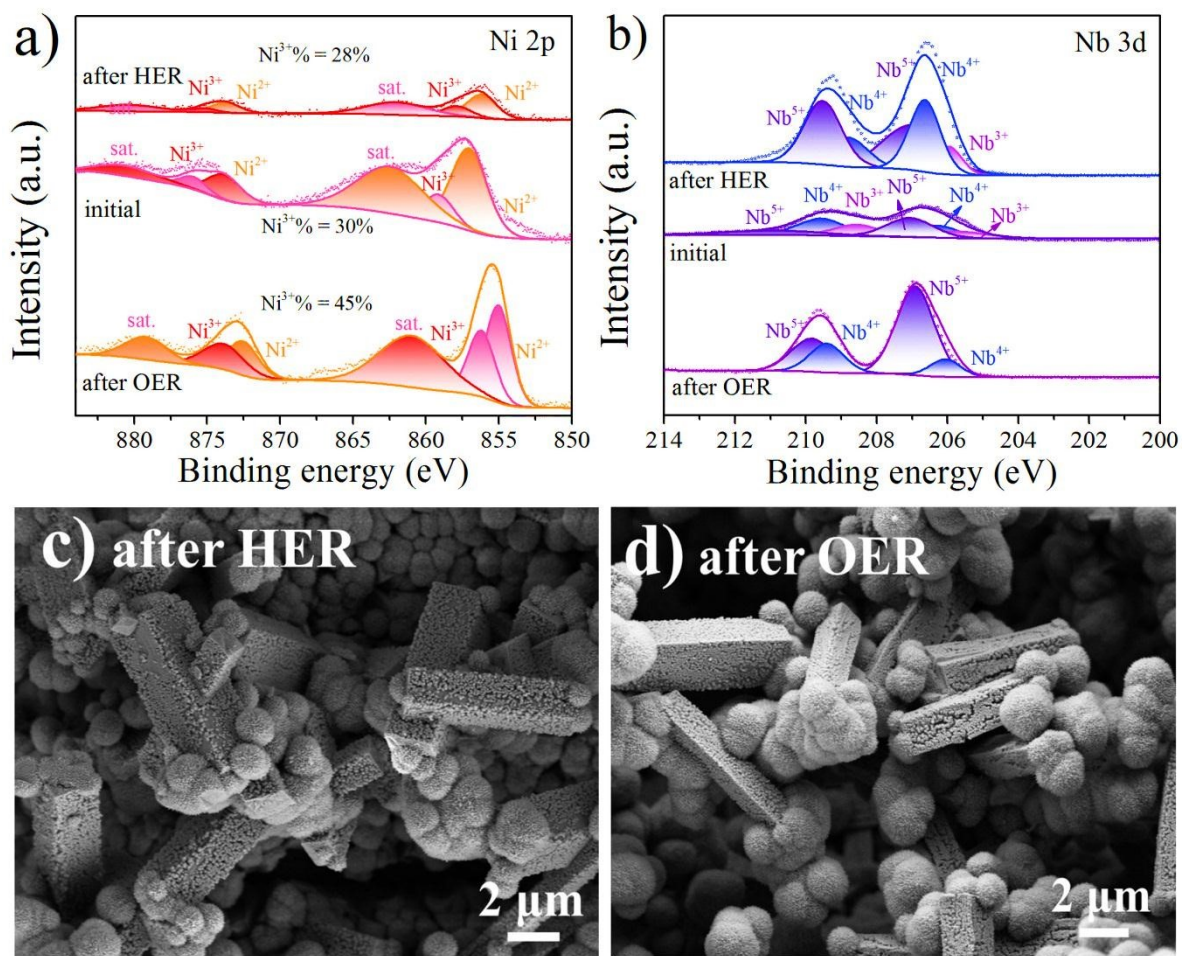
Fig. S16. XPS analysis comparison of SNiC$_2$O$_4$-Nb$_2$O$_5$ before and after the tests. a) Ni 2p, b) Nb 3d. SEM images of SNiC$_2$O$_4$-Nb$_2$O$_5$ after a) HER and b) OER test.
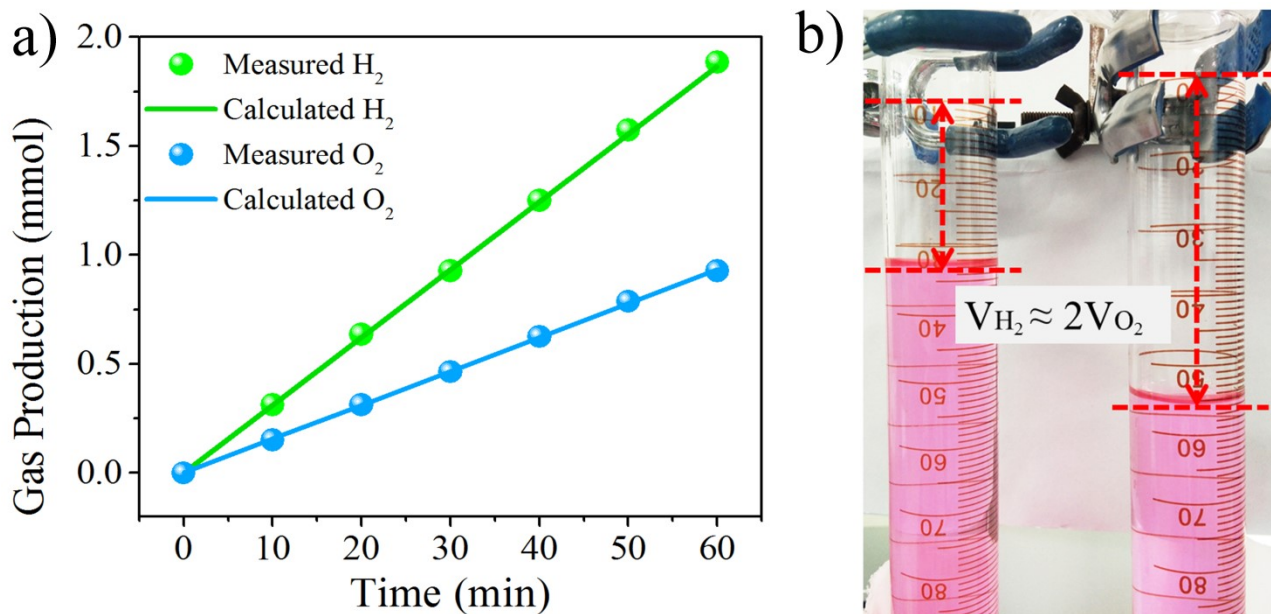
Fig. S17. (a) Experimental and theoretical amounts of H_2 and O_2 at a fixed current density of 100 mA cm^{-2} for SNiC$_2$O$_4$-Nb$_2$O$_5$/NF. (b) Optical picture of the collected H_2 and O_2 by water drainage method.
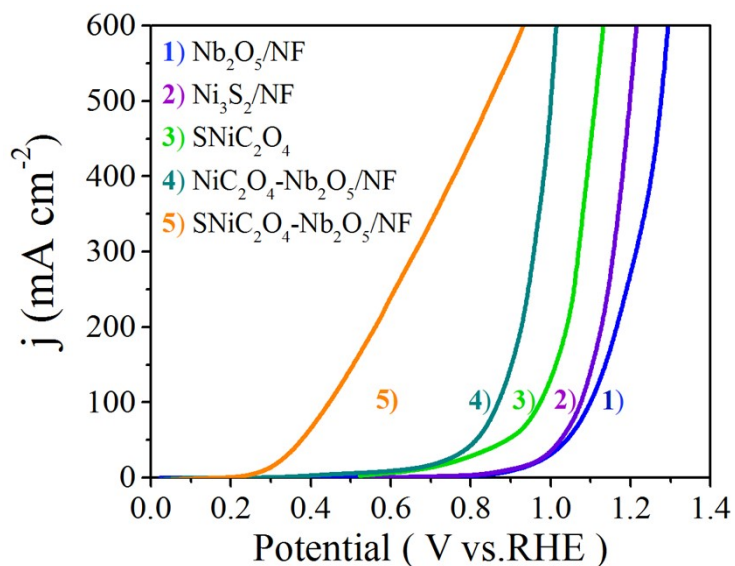
Fig. S18. LSV curves of Nb$_2$O$_5$, Ni$_3$S$_2$, SNiC$_2$O$_4$, NiC$_2$O$_4$-Nb$_2$O$_5$ and SNiC$_2$O$_4$-Nb$_2$O$_5$ grown on NF towards HzOR.
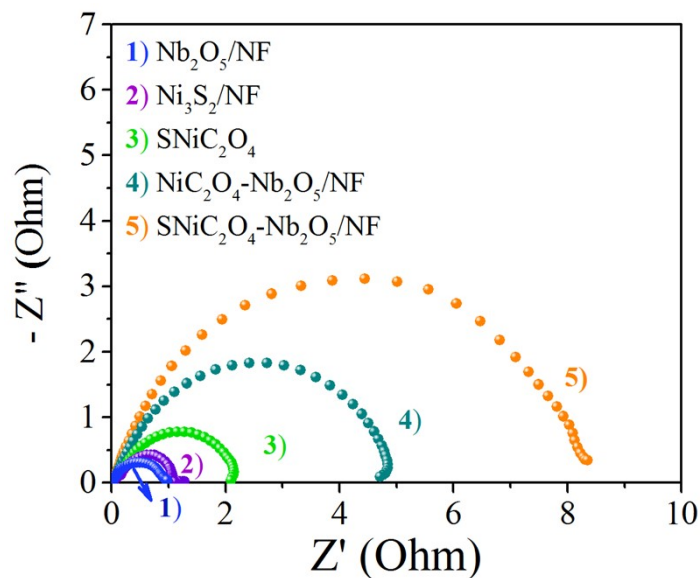
Fig. S19. EIS Nyquist plots of the as-prepared catalysts towards HzOR.
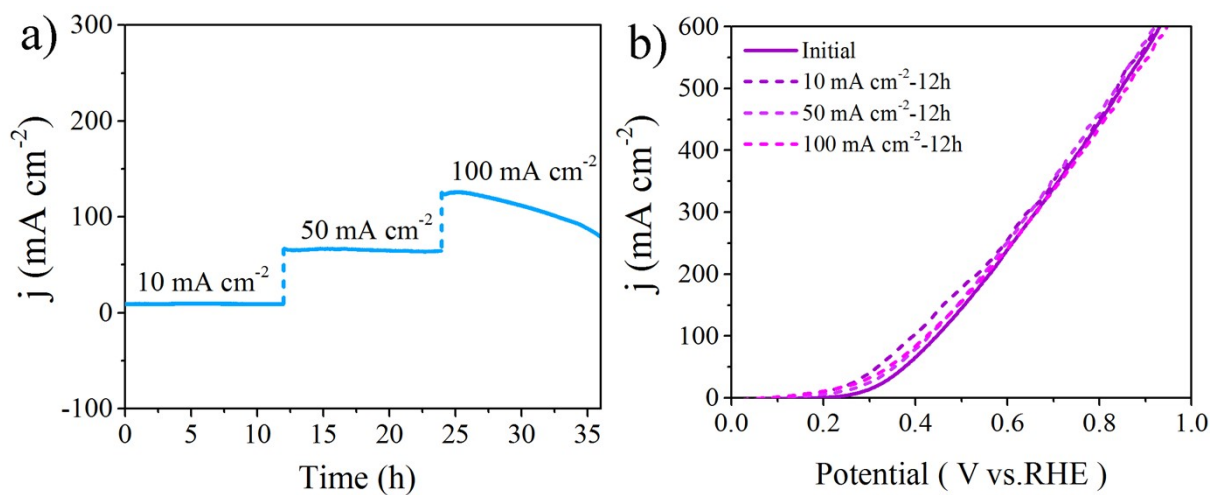
Fig. S20. a) Stability measurement of $SNiC_2O_4$-Nb_2O_5/NF at different current densities for 12 h. b) LSV curves of $SNiC_2O_4$-Nb_2O_5/NF before and after maintaining the current density at 10, 50, and 100 mA cm^{-2} for 12 h in HzOR. The polarization curves collected after the electrolyte is replaced.
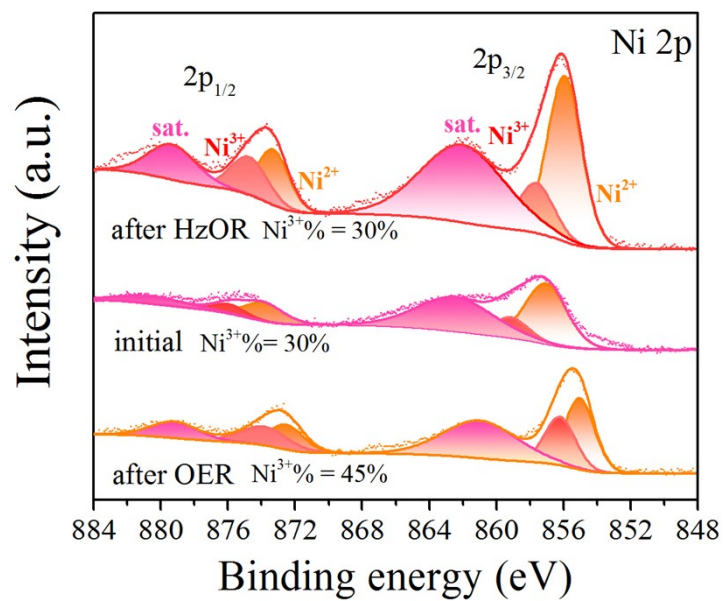
Fig. S21. Ni2p XPS spectral data of $SNiC_2O_4$-Nb_2O_5 before and after OER and HzOR tests.
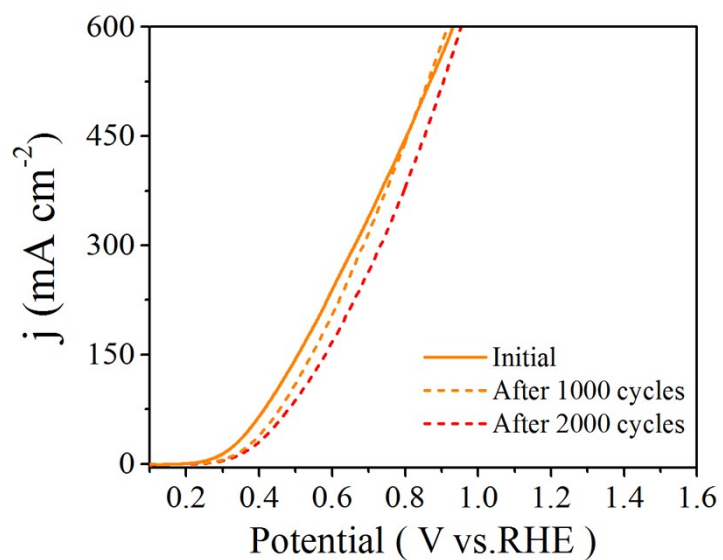
Fig. S22. Polarization curves of the $SNiC_2O_4$-Nb_2O_5/NF before and after 1000/2000 CV cycles for HzOR.
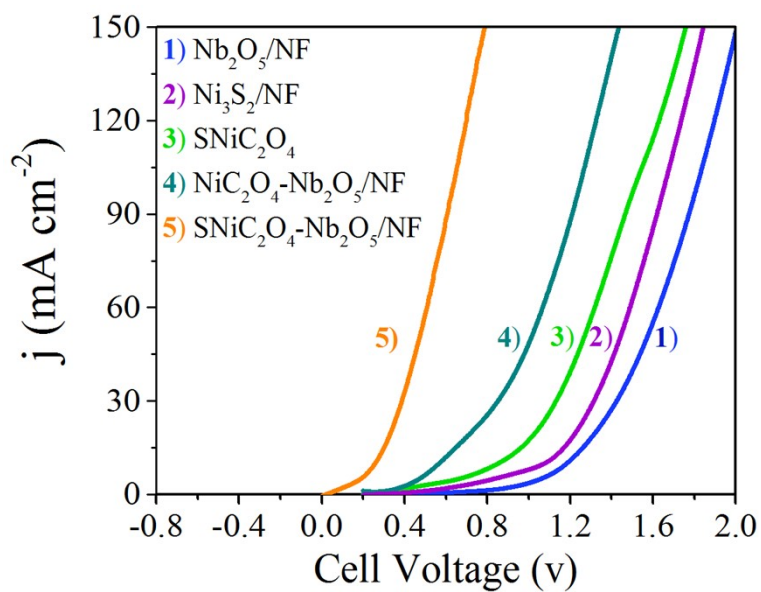
Fig. S23. LSV curves of Nb_2O_5, Ni_3S_2, $SNiC_2O_4$, NiC_2O_4-Nb_2O_5 and $SNiC_2O_4$-Nb_2O_5 grown on NF towards OHzS.
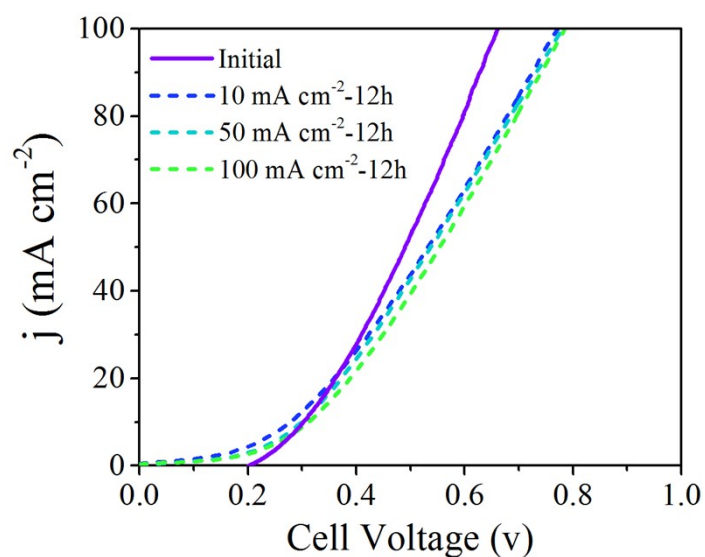
Fig. S24. LSV curves of $SNiC_2O_4$-Nb_2O_5/NF before and after maintaining the current density at 10, 50, and 100 mA cm^{-2} for 12 h in OHzS.
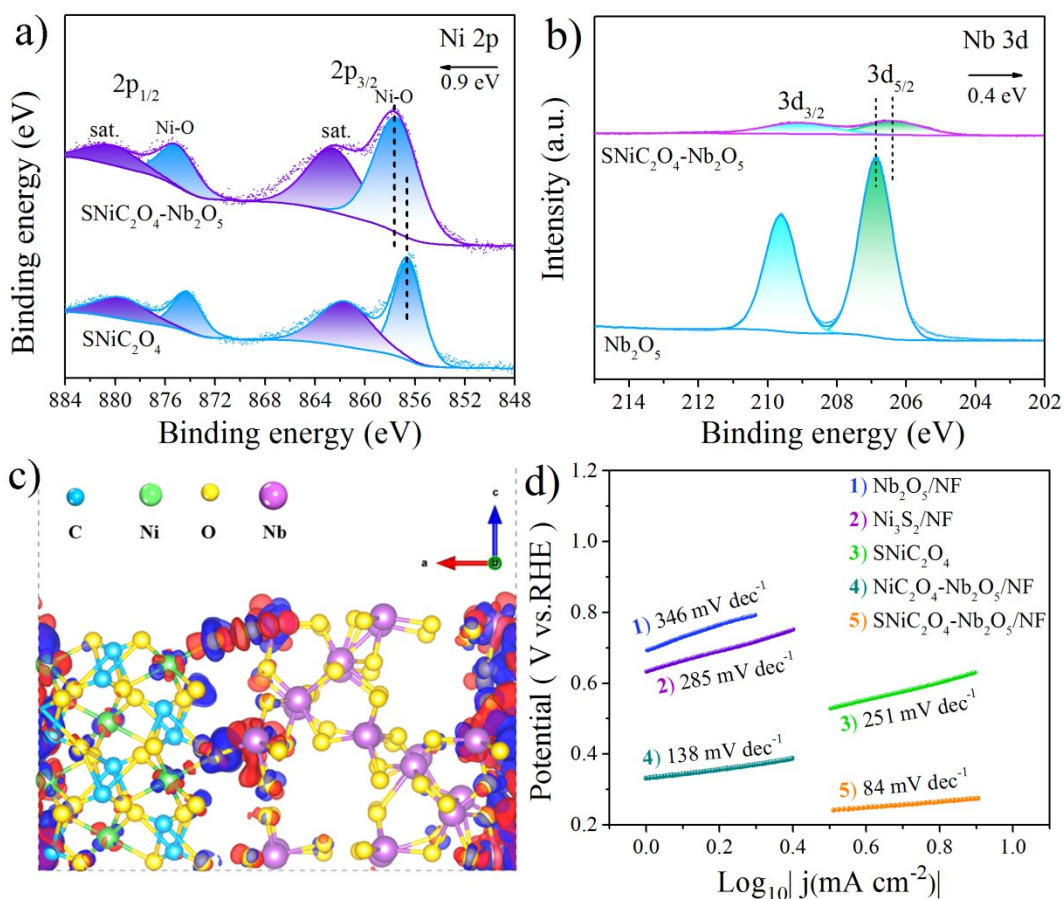
Fig. S25. Comparison of XPS spectral data of a) Ni and b) Nb for $SNiC_2O_4$-Nb_2O_5, $SNiC_2O_4$, and Nb_2O_5. c) The charge density difference of $SNiC_2O_4$-Nb_2O_5 with isosurface = 0.005 eV/Å^3 (red shadow: electron accumulation and blue shadow: electron depletion). d) Tafel slopes of Nb_2O_5, Ni_3S_2, $SNiC_2O_4$, NiC_2O_4-Nb_2O_5, and $SNiC_2O_4$-Nb_2O_5 grown on NF.
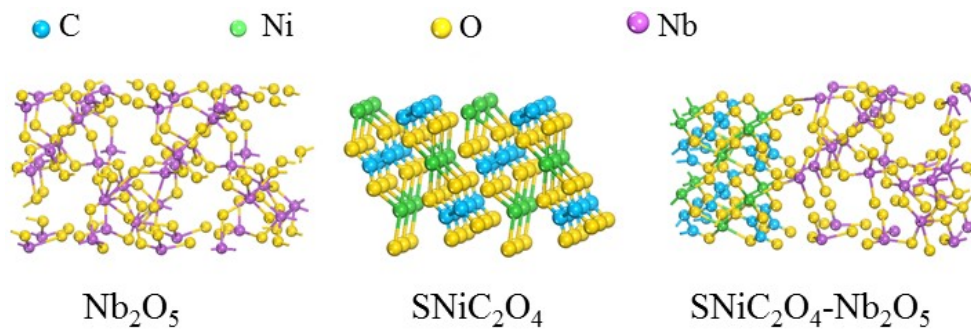
Fig. S26. Structural models of the Nb_2O_5, $SNiC_2O_4$, and $SNiC_2O_4$-Nb_2O_5.

a) Nb$_2$O$_5$ ● C ● Ni ○ O ● Nb

b) SNiC$_2$O$_4$

c) SNiC$_2$O$_4$-Nb$_2$O$_5$
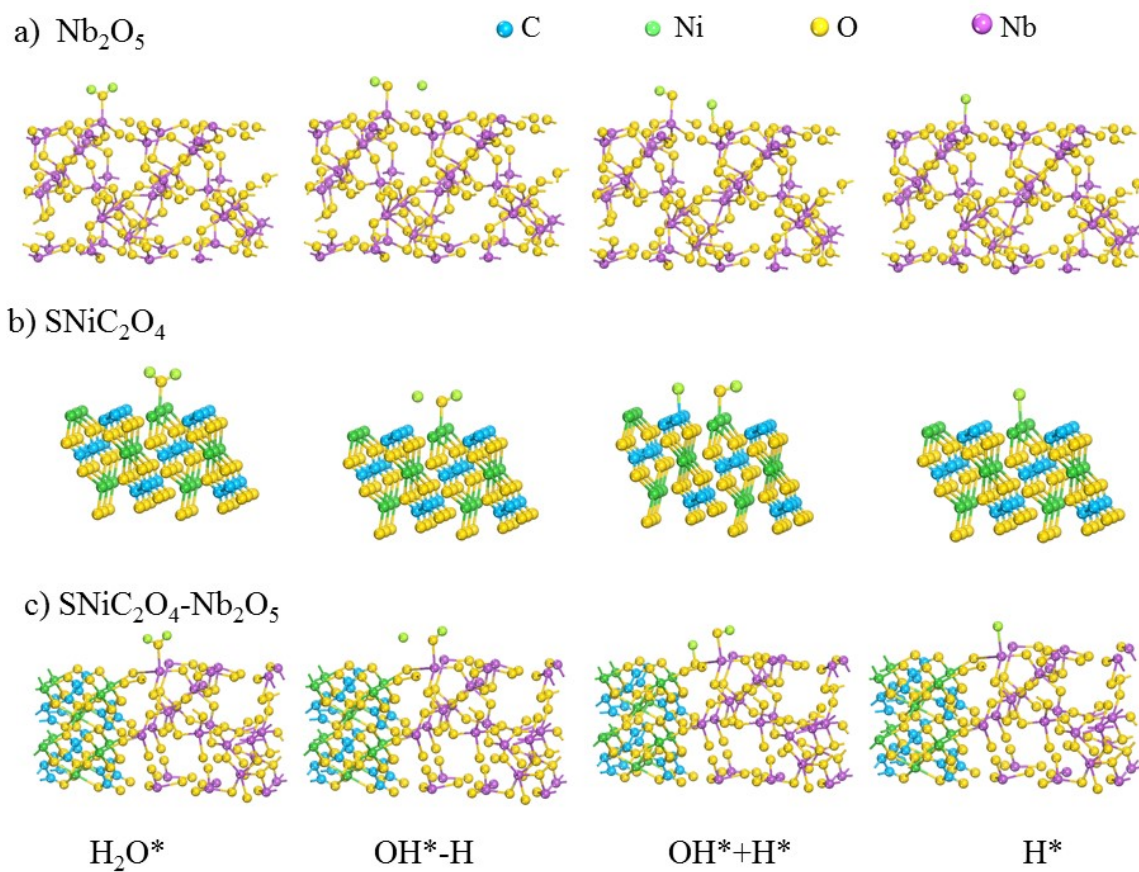
H$_2$O* OH*-H OH*+H* H*

Fig. S27. Optimized structure models of H$_2$O*, OH*-H, OH*+H* and H* adsorbed on a) Nb$_2$O$_5$, b) SNiC$_2$O$_4$, and c) SNiC$_2$O$_4$-Nb$_2$O$_5$.
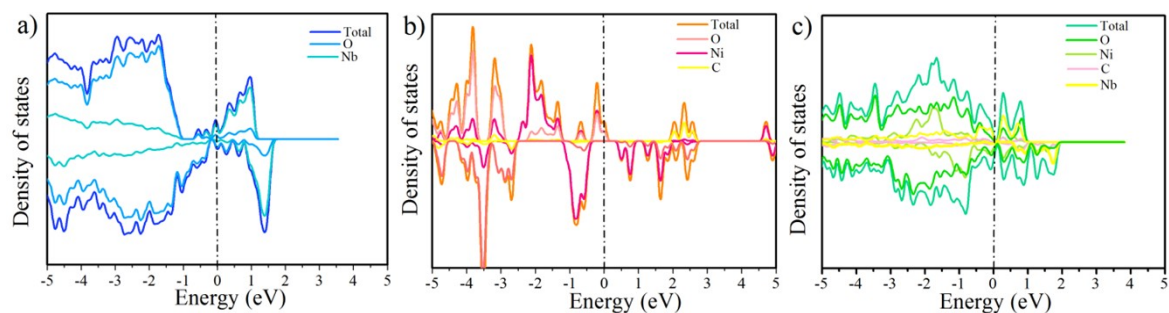
Fig. S28. Calculated DOS of a) Nb_2O_5, b) $SNiC_2O_4$, and c) $SNiC_2O_4$-Nb_2O_5.
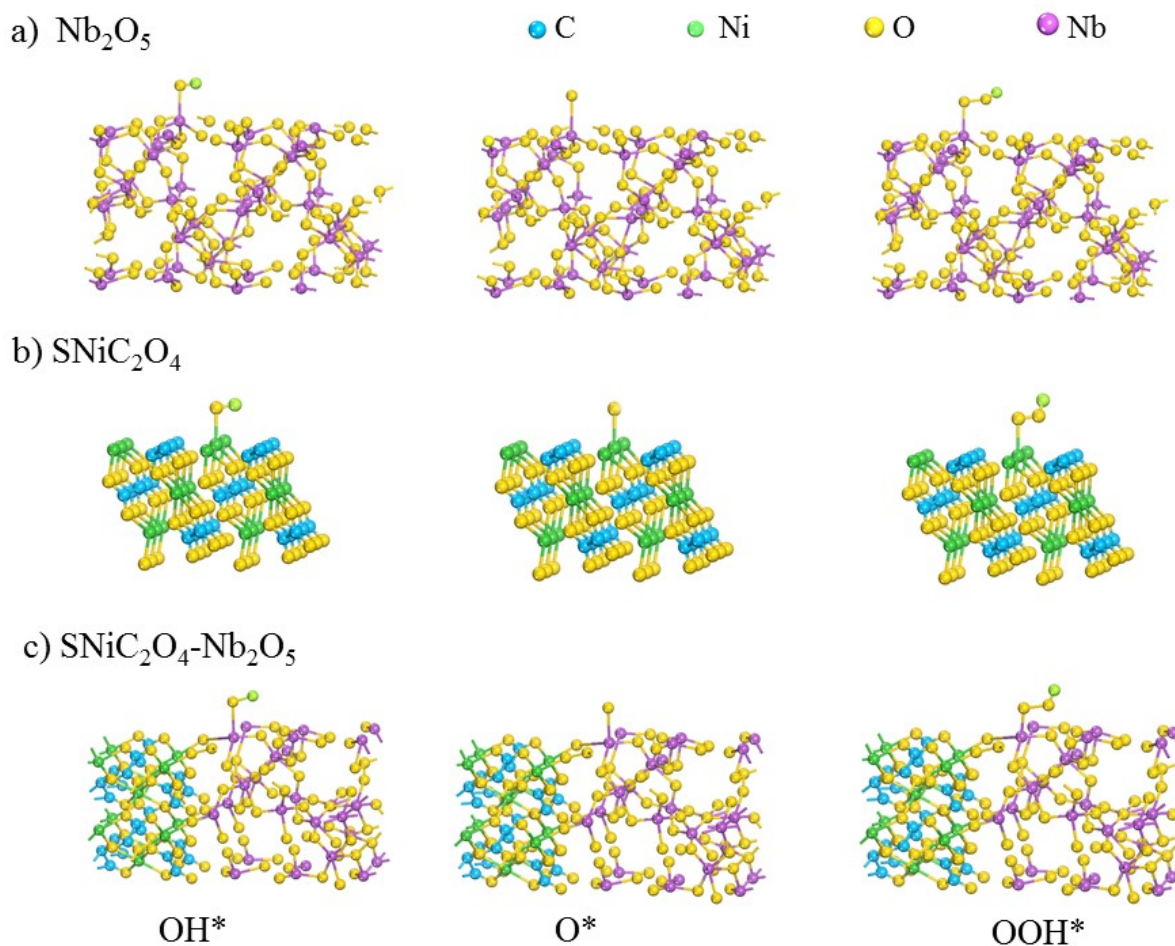
Fig. S29. Optimized structure models of a) Nb_2O_5, b) $SNiC_2O_4$ and c) $SNiC_2O_4$-Nb_2O_5 for adsorption of intermediates (OH*, O*, and OOH*) under OER in an alkaline medium.

Table S3. Comparison of electrocatalytic activity for HER of this work with other non-noble metal catalysts in 1.0 M KOH solution.

Catalyst	Substrate	Overpotential	Reference
NiCo hybrid	Glassy carbon	353 mV@10 mA cm^{-2}	[10]
CoP$_3$ NAs[a]	Carbon fiber paper	165 mV@10 mA cm^{-2}	[11]
Ni$_3$S$_2$	Ni foam	170 mV@10 mA cm^{-2}	[12]
CoP	Glassy carbon	178 mV@10 mA cm^{-2}	[13]
FeP	Carbon cloth	202 mV@10 mA cm^{-2}	[14]
Fe-NiC$_2$O$_4$	Ni foam	151 mV@10 mA cm^{-2}	[15]
NiS	Ni foam	158 mV@20 mA cm^{-2}	[16]
NiCo$_2$S$_4$	Carbon cloth	190 mV@20 mA cm^{-2}	[17]
Ni$_2$P	Glassy carbon	255 mV@20 mA cm^{-2}	[18]
Co$_3$N	Cobalt plate	275 mV@20 mA cm^{-2}	[19]
Ni(OH)$_2$ nanosheets	Ni foam	172 mV@20 mA cm^{-2}	[20]
Ni$_2$P	Ni foam	255 mV@20 mA cm^{-2}	[18]
Ni$_{1-x}$Fe$_x$-LDH[b]	Ni foam	319 mV@50 mA cm^{-2}	[21]
Co$_{1-x}$Fe$_x$-LDH	Ni foam	273 mV@50 mA cm^{-2}	[21]
NiCo$_2$S$_4$ NS[c]	Carbon cloth	266 mV@50 mA cm^{-2}	[22]
Co$_{0.75}$Ni$_{0.25}$Se	Ni foam	269 mV@50 mA cm^{-2}	[23]
SNiC$_2$O$_4$-Nb$_2$O$_5$	Ni foam	125 mV@10 mA cm^{-2} 155 mV@20 mA cm^{-2} 195 mV@50 mA cm^{-2}	This work

a) NAs: nanoneedle arrays; b) LDH: layered-double-hydroxide; c) NS: nanosheet

Table S4. Comparison of electrocatalytic activity for OER of this work with other non-noble metal catalysts in 1.0 M KOH solution.

Catalyst	Substrate	Overpotential	Reference
CoC_2O_4	Glassy carbon	348 mV@10 mA cm^{-2}	[24]
Ni_5P_4	Ni foil	470 mV@10 mA cm^{-2}	[25]
$Ni@[Ni^{(2+/3+)}Co_2(OH)_{6-7}]_x$	ITO[a] electrode	460 mV@10 mA cm^{-2}	[26]
α-CoOOH	Glassy carbon	320 mV@10 mA cm^{-2}	[27]
α-Ni(OH)$_2$	Glassy carbon	331 mV@10 mA cm^{-2}	[28]
$Ni_{0.7}Fe_{0.3}S_2$	Ni foam	355 mV@20 mA cm^{-2}	[29]
NiFe LDH[b]	Ni foam	330 mV@20 mA cm^{-2}	[30]
NiFeP/CoP	Carbon cloth	250 mV@20 mA cm^{-2}	[31]
$Ni_{0.2}Mo_{0.8}N/Fe-Ni_3N$	Ni foam	266 mV@20 mA cm^{-2}	[32]
Fe rusts/Ni(OH)$_2$	Fe foam	318 mV@20 mA cm^{-2}	[33]
W_2N/WC	Ni foam	320 mV@20 mA cm^{-2}	[34]
$Ni_{1-x}Fe_x$-LDH	Ni foam	300 mV@50 mA cm^{-2}	[21]
NiFe LDH	microwave-reduced GO[c]	335 mV@50 mA cm^{-2}	[35]
Ni-P	Cu foam	410 mV@50 mA cm^{-2}	[36]
NiMo HNRs[d]	Ti mesh	344 mV@50 mA cm^{-2}	[37]
CoSe	Ti mesh	341 mV@50 mA cm^{-2}	[38]
NiSe@NiOOH	Ni foam	332 mV@50 mA cm^{-2}	[39]
CoP	Ni foam	319 mV@50 mA cm^{-2}	[40]
$SNiC_2O_4-Nb_2O_5$	Ni foam	293 mV@20 mA cm^{-2} 360 mV@50 mA cm^{-2}	This work

a) ITO: indium tin oxide; b) LDH: layered-double-hydroxide; c) GO: graphene oxide; d) HNRs: hollow nanorod arrays.

Table S5. The content of the corresponding valence states of Ni and Nb in $SNiC_2O_4$-Nb_2O_5 before and after the test.

Catalyst	Ni^{2+}/%	Ni^{3+}/%	Nb^{3+}/%	Nb^{4+}/%	Nb^{5+}/%
initial	72	30	26	37	37
after HER	75	25	8	36	56
after OER	55	45	-	25	75

The corresponding data were obtained from the XPS spectra, and the content of the valence states is calculated by the following formula:

$$Ni^{2+} = Ni^{2+} / (Ni^{2+} + Ni^{3+}) \qquad\qquad \text{Eq. (11)}$$

$$Ni^{3+} = Ni^{3+} / (Ni^{2+} + Ni^{3+}) \qquad\qquad \text{Eq. (12)}$$

$$Nb^{3+} = Nb^{3+} / (Nb^{3+} + Nb^{4+} + Nb^{5+}) \qquad\qquad \text{Eq. (13)}$$

$$Nb^{4+} = Nb^{4+} / (Nb^{3+} + Nb^{4+} + Nb^{5+}) \qquad\qquad \text{Eq. (14)}$$

$$Nb^{5+} = Nb^{5+} / (Nb^{3+} + Nb^{4+} + Nb^{5+}) \qquad\qquad \text{Eq. (15)}$$

Table S6. Comparison of electrocatalytic activity for overall water splitting of this work with other non-noble metal catalysts in 1.0 M KOH solution.

Catalyst	Substrate	Cell voltage	Reference
$Ni_{0.5}Co_{0.5}/NC^a$	N-carbon films	1.75 V@10 mA cm^{-2}	[41]
Co_3O_4/N-doped carbon	Ni foam	1.74 V@10 mA cm^{-2}	[42]
$SrTi_{0.1}Fe_{0.85}Ni_{0.05}O_{3-\delta}$	Ni foam	1.80 V@10 mA cm^{-2}	[43]
Co-ZnO nanowires	Cu foam	2.01 V@10 mA cm^{-2}	[44]
$S-NiFe_2O_4$	Ni foam	1.95 V@10 mA cm^{-2}	[45]
$Co@Co_3O_4$	Ni foam	2.00 V@10 mA cm^{-2}	[46]
Ni foam	Ni foam	2.00 V@10 mA cm^{-2}	[47]
Co-S/Carbon tube	Carbon paper	1.74 V@10 mA cm^{-2}	[48]
NiFe@NC	Ni foam	1.81 V@10 mA cm^{-2}	[49]
Vanadium nanobelts	Ni foam	1.74 V@10 mA cm^{-2}	[50]
$NiFeO_x$	Carbon nanofibres	1.88 V@10 mA cm^{-2}	[51]
$Ni(OH)_2$/NiSe	Carbon paper	1.78 V@10 mA cm^{-2}	[52]
$Ni_{12}P_5/Ni_3(PO_4)_2$	Ni foam	1.76 V@10 mA cm^{-2}	[53]
Co-P film	Au foil	1.73 V@10 mA cm^{-2}	[54]
FeCoNi	Carbon cloth	1.67 V@10 mA cm^{-2}	[55]
$SNiC_2O_4-Nb_2O_5$	Ni foam	1.66 V@10 mA cm^{-2} 1.74 V@20 mA cm^{-2}	This work

a) NC: nitrogen-doped carbon

References

1. G. Kresse and J. Furthmüller, *Phys. Rev. B*, 1996, **54**, 11169-11186.

2. J. P. Perdew, K. Burke and M. Ernzerhof, *Phys. Rev. Lett.*, 1996, **77**, 3865-3868.

3. G. Kresse and D. Joubert, *Phys. Rev. B*, 1999, **59**, 1758-1775.

4. P. E. Blöchl, *Phys. Rev. B*, 1994, **50**, 17953-17979.

5. S. Grimme, J. Antony, S. Ehrlich and H. Krieg, *J. Chem. Phys.*, 2010, **132**, 154104.

6. G. Henkelman, B. P. Uberuaga and H. Jónsson, *J. Chem. Phys.*, 2000, **113**, 9901-9904.

7. Y. Yan, J.-Y. Zhang, X.-R. Shi, Y. Zhu, C. Xia, S. Zaman, X. Hu, X. Wang and B. Y. Xia, *ACS Nano*, 2021, **15**, 10286-10295.

8. Y. Liu, J. Zhang, Y. Li, Q. Qian, Z. Li and G. Zhang, *Adv. Funct. Mater.*, 2021, **31**, 2103673.

9. Q. Qian, J. Zhang, J. Li, Y. Li, X. Jin, Y. Zhu, Y. Liu, Z. Li, A. El-Harairy, C. Xiao, G. Zhang and Y. Xie, *Angew. Chem. Int. Ed.*, 2021, **60**, 5984-5993.

10. J. Saha, R. Ball and C. Subramaniam, *ACS Sustainable Chem. Eng.*, 2021, **9**, 7792-7802.

11. T. Wu, M. Pi, D. Zhang and S. Chen, *J. Mater. Chem. A,* 2016, **4**, 14539-14544.

12. L.-L. Feng, G. Yu, Y. Wu, G.-D. Li, H. Li, Y. Sun, T. Asefa, W. Chen and X. Zou, *J. Am. Chem. Soc.*, 2015, **137**, 14023-14026.

13. J. Ma, M. Wang, G. Lei, G. Zhang, F. Zhang, W. Peng, X. Fan and Y. Li, *Small*, 2018, **14**, 1702895.

14. Y. Liang, Q. Liu, A. M. Asiri, X. Sun and Y. Luo, *ACS Catal.*, 2014, **4**, 4065-4069.

15. X. Wang, P. He, Y. Yang, F. Zhang, J. Tang and R. Que, *Electrochim. Acta*, 2020, **345**, 136228.

16. W. Zhu, X. Yue, W. Zhang, S. Yu, Y. Zhang, J. Wang and J. Wang, *Chem. Commun.*, 2016, **52**, 1486-1489.

17. D. Liu, Q. Lu, Y. Luo, X. Sun and A. M. Asiri, *Nanoscale*, 2015, **7**, 15122-15126.

18. L.-A. Stern, L. Feng, F. Song and X. Hu, *Energy Environ. Sci.*, 2015, **8**, 2347-2351.

19. Z. Xu, W. Li, Y. Yan, H. Wang, H. Zhu, M. Zhao, S. Yan and Z. Zou, *ACS Appl. Mater. Interfaces*, 2018, **10**, 22102-22109.

20. Y. Rao, Y. Wang, H. Ning, P. Li and M. Wu, *ACS Appl. Mater. Interfaces*, 2016, **8**, 33601-33607.

21. G. Rajeshkhanna, T. I. Singh, N. H. Kim and J. H. Lee, *ACS Appl. Mater. Interfaces*, 2018, **10**,

42453-42468.

22. R. Zhang, R. Hu, X. Li, Z. Zhen, Z. Xu, N. Li, L. He and H. Zhu, *Adv. Funct. Mater.*, 2018, **28**, 1705879.

23. S. Liu, Y. Jiang, M. Yang, M. Zhang, Q. Guo, W. Shen, R. He and M. Li, *Nanoscale*, 2019, **11**, 7959-7966.

24. X. Liu, J. Jiang and L. Ai, *J. Mater. Chem. A,* 2015, **3**, 9707-9713.

25. M. Ledendecker, S. Krick Calderón, C. Papp, H.-P. Steinrück, M. Antonietti and M. Shalom, *Angew. Chem. Int. Ed.*, 2015, **54**, 12361-12365.

26. Z. Zhao, H. Wu, H. He, X. Xu and Y. Jin, *Adv. Funct. Mater.*, 2014, **24**, 4698-4705.

27. P. F. Liu, S. Yang, L. R. Zheng, B. Zhang and H. G. Yang, *J. Mater. Chem. A,* 2016, **4**, 9578-9584.

28. M. Gao, W. Sheng, Z. Zhuang, Q. Fang, S. Gu, J. Jiang and Y. Yan, *J. Am. Chem. Soc.*, 2014, **136**, 7077-7084.

29. J. Yu, G. Cheng and W. Luo, *J. Mater. Chem. A,* 2017, **5**, 15838-15844.

30. J. Luo, J.-H. Im, M. T. Mayer, M. Schreier, M. K. Nazeeruddin, N.-G. Park, S. D. Tilley, H. J. Fan and M. Grätzel, *Science*, 2014, **345**, 1593.

31. X. Jiang, Y. Li, M. He, L. Zhou, Q. Zheng, F. Xie, W. Jie and D. Lin, *Int. J. Hydrogen Energy*, 2019, **44**, 19986-19994.

32. C. Liu, H. Zhu, S. Lu, F. Xu, F. Duan and M. Du, *RSC Adv.*, 2021, **11**, 19797-19804.

33. X. Liu, X. Guo, M. Gong, S. Deng, J. Liang, T. Zhao, Y. Lu, Y. Zhu, J. Zhang and D. Wang, *Electrochim. Acta*, 2020, **353**, 136478.

34. J. Diao, Y. Qiu, S. Liu, W. Wang, K. Chen, H. Li, W. Yuan, Y. Qu and X. Guo, *Adv.Mater.*, 2020, **32**, 1905679.

35. D. Voiry, J. Yang, J. Kupferberg, R. Fullon, C. Lee, H. Y. Jeong, H. S. Shin and M. Chhowalla, *Science*, 2016, **353**, 1413.

36. Q. Liu, S. Gu and C. M. Li, *Journal of Power Sources*, 2015, **299**, 342-346.

37. J. Tian, N. Cheng, Q. Liu, X. Sun, Y. He and A. M. Asiri, *J. Mater. Chem. A,* 2015, **3**, 20056-20059.

38. T. Liu, Q. Liu, A. M. Asiri, Y. Luo and X. Sun, *Chem. Commun.*, 2015, **51**, 16683-16686.

39. X. Li, G.-Q. Han, Y.-R. Liu, B. Dong, W.-H. Hu, X. Shang, Y.-M. Chai and C.-G. Liu, *ACS*

Appl. Mater. Interfaces, 2016, **8**, 20057-20066.

40. G. Li, L. Li and Z. Lin, *Int. J. Hydrogen Energy*, 2021, **46**, 18224-18232.

41. B. Bayatsarmadi, Y. Zheng, V. Russo, L. Ge, C. S. Casari and S.-Z. Qiao, *Nanoscale*, 2016, **8**, 18507-18515.

42. B. Wang, L. Xu, G. Liu, P. Zhang, W. Zhu, J. Xia and H. Li, *J. Mater. Chem. A,* 2017, **5**, 20170-20179.

43. X. Wu, J. Yu, G. Yang, H. Liu, W. Zhou and Z. Shao, *Electrochim. Acta*, 2018, **286**, 47-54.

44. G. Li, X. Wang, M. H. Seo, S. Hemmati, A. Yu and Z. Chen, *J. Mater. Chem. A,* 2017, **5**, 10895-10901.

45. J. Liu, D. Zhu, T. Ling, A. Vasileff and S.-Z. Qiao, *Nano Energy*, 2017, **40**, 264-273.

46. C. Bai, S. Wei, D. Deng, X. Lin, M. Zheng and Q. Dong, *J. Mater. Chem. A,* 2017, **5**, 9533-9536.

47. Y. Zhu, W. Zhou, Y. Zhong, Y. Bu, X. Chen, Q. Zhong, M. Liu and Z. Shao, *Adv. Energy Mater.*, 2017, **7**, 1602122.

48. J. Wang, H.-x. Zhong, Z.-l. Wang, F.-l. Meng and X.-b. Zhang, *ACS Nano*, 2016, **10**, 2342-2348.

49. Z. Zhang, Y. Qin, M. Dou, J. Ji and F. Wang, *Nano Energy*, 2016, **30**, 426-433.

50. Y. Yu, P. Li, X. Wang, W. Gao, Z. Shen, Y. Zhu, S. Yang, W. Song and K. Ding, *Nanoscale*, 2016, **8**, 10731-10738.

51. H. Wang, H.-W. Lee, Y. Deng, Z. Lu, P.-C. Hsu, Y. Liu, D. Lin and Y. Cui, *Nat. Commun.*, 2015, **6**, 7261.

52. H. Liang, L. Li, F. Meng, L. Dang, J. Zhuo, A. Forticaux, Z. Wang and S. Jin, *Chem. Mater.*, 2015, **27**, 5702-5711.

53. A. Sivanantham and S. Shanmugam, *Appl. Catal. B Environ.*, 2017, **203**, 485-493.

54. J. A. Vigil and T. N. Lambert, *RSC Adv.*, 2015, **5**, 105814-105819.

55. Y. Yang, Z. Lin, S. Gao, J. Su, Z. Lun, G. Xia, J. Chen, R. Zhang and Q. Chen, *ACS Catal.*, 2017, **7**, 469-479.